Dual Carrier Preparations for Viking

D. A. Bathker
Communications Elements Research Section

D. W. Brown
R. F. Systems Development Section

The problem of receive band interference resulting from both single and dual carrier transmission from a deep space station has been synthesized and, to a large extent, resolved at the Venus Deep Space Station. Although there are remaining problems, the application of this experience to 64-m-diam antenna stations, the Mars Deep Space Station in particular, is discussed.

I. Introduction

Receive band interference resulting from high power diplexing with dual carrier uplink has been the subject of intensive investigation in recent months. A description of the problem was given in a recent report (Ref. 1) along with a brief summary and references to background experience and related work. This report will be more specific; a review of DSS 14 performance will be given as well as related progress achieved at DSS 13 (Refs. 2, 3) through the end of calendar 1972.

II. Description

The interference consists of two types: (1) broadband noise bursts (NB) which occur with single *or* dual carrier transmission and are observed as impulsive increases in receiving system temperature and, (2) intermodulation products (IMPs) whose frequencies may be predicted by the expression:

$$F_{IMP} = (N + 1) F_2 - NF_1$$

where F_2 and F_1 represent the upper and lower uplink carrier frequencies and N takes positive integral values. The intermodulation order (IO) is defined as the sum of the absolute values of the coefficients above, that is:

$$IO = 2N + 1$$

However, for convenience, the first expression may be written as:

$$F_{IMP} = F_2 + N(F_2 - F_1)$$

where N is clearly the index of the Nth spectral line at interval $(F_2 - F_1)$ appearing above the upper carrier frequency F_2.

Because the DSN receive band (2290 to 2300 MHz) lies at a more or less fixed interval (180 MHz) above the transmit band (2110 to 2120 MHz) in the spacecraft transponder ratio of 240/221, it is apparent that the value or values of N appearing in the receive band may be approximated as follows:

$$N_{rcv} = \frac{180 \pm 5\,\text{MHz}}{(F_2 - F_1)}$$

For instance, if the uplink channel separation were 6 MHz, one would expect N = 30 (as well as 29 and possibly 31) to appear within the receive band. Indeed, this is the case, and for each pair of the four Viking channel assignments (9, 13, 16, 20), the representative indices are N = 48 (channels 9, and 20), 75 (channels 9 and 16 or 13 and 20), 133 (channels 9 and 13 or 16 and 20) and 175 (channels 13 and 16). Although none of the several IMPs falling in the receive band may lie within an active receive channel for a particular pair of uplink frequencies, these IMPs will walk through the receive band as N times the differential uplink tuning, and thereby impact any and all receive channels as the uplinks are operationally tuned as a function of uplink doppler.

Experience has shown that, while these IMPs are entirely predictable regarding center frequency, they appear to have a spectral width of 10 Hz or so, as if modulated by the random noise burst effect. The overall interference then appears throughout the receive band with clusters of noise energy at the IMP frequencies. In fact, recordings of the usual instrumentation—receiving system temperature (T_{op}) and receiver AGC voltage—show a strong correlation in time between the magnitude and time density of noise bursts and the AGC estimate of IMP power. This is especially true in the short term (seconds), but also generally true in medium (minutes) or long (hours, days) term. Similarly, the noise burst activity and IMP effect appear to be somewhat correlated in magnitude as a function of system condition as if they both arise from the same basic mechanisms (microarcs or other nonlinearities). And yet, there are some clues that internal waveguide mechanisms may generate noise bursts in somewhat weaker proportion to the IMP mean than do external antenna sources. One clue to support this view is the observation that, while operating in an internal mode (without the antenna), the IMP is characterized as having less AGC voltage variance, for a given mean, than a complete antenna system.

III. Review of DSS 14 Performance

Considering for a moment the uplink low-order (N = 1, 2) intermodulation products generated primarily in the klystron, the aforementioned Viking channels were selected such that these IMPs would not fall within an assigned uplink channel. In addition, the power per carrier has been nominally established at 10% of single carrier klystron rating (Ref. 4), in order to limit the uplink IMPs to at least 20 dB below each carrier as based upon tests early in 1972 (Ref. 5). This results in dual 40-kW nominal capability at DSS 14 and dual 10-kW rating at DSS 13 and overseas 64-m-diam antenna stations.

Early concerns regarding suspected receive band interference in the Viking mode led to preliminary testing at DSS 14 with carrier separations yielding values of N as low as 31 and as high as 75. First results showed mean values of receiver AGC (when locked to the IMP) to be typically −140 dBmW for N = 31, somewhat weaker values for N as high as 45, and no lock for the higher values of N. These data suggested a model of monotonically weaker IMPs for increasing N, with the projection of near threshold (and therefore potentially degrading) interference at least for N = 48 and possibly for N = 75 in the Viking mode. Repeated testing confirmed this by demonstrating N = 48 receiver locks with IMP means in the vicinity of −168 dBmW. The full significance of these values has not yet been established, but any consideration of these mean levels of IMP must recognize the short-term fluctuations which have been typically ±10 dB for 0.1 Hz AGC bandwidth (narrow) and perhaps as much as ±20 dB for wide AGC bandwidth. Figure 1 presents typical mean values of IMP for several values of N and attempts to depict the medium- and long-term variations as well. During these tests, noise burst activity was typically of the order of 100 K peaks and, for a given system condition, was consistently more noisy for dual 40 kW than for single carrier powers of 100 to 400 kW. The reason for dual carriers being more effective than a single carrier of equal or greater power level in stimulating noise bursts is not understood. The effectiveness is consistently evident in both amplitude and time density of the noise bursts.

While examining potential tradeoffs and clues to the IMP behavior, several attempts were made to evaluate mean IMP levels as a function of transmitted power per carrier. Incidental equipment problems as well as medium term variations have clouded the result. Figure 2 depicts some of the data which suggest a possible 3-dB IMP per dB of balanced transmitter power relationship. Whether

or not this is true and whether or not operational use of this effect could be exploited depends strongly upon certain assumptions and conditions of medium term fluctuation of the IMP at a given power level.

IV. DSS 13 Dual Carrier Implementation and Performance

Although the Viking dual carrier commitment (Ref. 1) specifies 64-m station support, any major effort in terms of extensive experimentation with dual carriers at a 64-m station would be extremely difficult. In the past, significant single carrier noise burst and dual carrier (restricted to uplink intermodulation product) testing had been accomplished at the Goldstone DSCC Microwave Test Facility (MTF) and Venus (DSS 13) 26-m Deep Space Station (Refs. 6, 7). Early in June 1972, a management decision was made which would significantly impact DSS 13. The obvious needs of typical DSN antenna reflecting surfaces, together with a 100- to 400-kW class transmitter and low noise receiver could be most easily achieved by committing DSS 13 to a dual carrier test program. The results and conclusions obtained from that program could then be assessed with regard to impact upon the 64-m network.

Considerable planning was required to outfit DSS 13 with a dual carrier test capability, both in terms of the capability itself, and ancillary test features such as observation ports, air and water terminations and the like. Figure 3 shows the block diagram arrived at after much consultation among various groups involved. A 100-kW klystron was made available. It is interesting to note, for the nominal dual 10-kW carriers, that the power density incident on a 26-m antenna is comparable to dual 40-kW carriers on the DSS 14 64-m-diam antenna. Standard 400-kW DSN filtering was made available from 64-m network spares. Initially a Block II traveling wave maser (TWM) was made available as preamplifier for the DSS 13 receiver. Receivers in use at DSS 13 included the 2295-MHz R&D receiver operated both open loop and 455 kHz closed loop. Open-loop T_{op} instrumentation was available with 1-MHz bandwidth. The XDS 930 computer was used as a digital spectrum analyzer. A low-noise transistorized preamplifier was used with an analog spectrum analyzer (LNSA), for example, to examine receive band IMPs, if any, directly from the klystron or from the test probes. A high-power waveguide directional coupler was available to sample forward and reverse transmitter power over a broad band. Four terminations were initially selected; the complete 26-m antenna with S-band Radar Operational (SRO) feedcone, the 26-m antenna SRO feedcone without antenna, by way of a flat plate reflector over the feedhorn, a water load, and an air load termed side-looking horn (SLH). A view of the DSS 13 side-looking horn installation is seen in Fig. 4. This termination provides the simplest possible radiator, closely coupled in terms of numbers of waveguide flanges to the transmitter/filtering/receiver system, housed within the DSS 13 26-m antenna electronics room seen in the upper portion of Fig. 4.

Additional work accomplished at this time (September 1972) was to remove all questionably bonded hardware from the exterior reflecting surfaces of the DSS 13 26-m antenna. This hardware included conduits, lights, clamps, ladders, and other peripheral equipment. The reflecting surface was completely retaped using newly available corner patches, as seen in Fig. 5. Also shown in Fig. 5 are the two surface probes seen in the block diagram (Fig. 3). One probe is broadband (waveguide bandwidth) while the other is a highpass filter, cutoff at 2200 MHz. With it, the receive band can be observed without simultaneously coupling in the strong transmitted signals near 2115 MHz.

Figure 6 shows the DSS 13 antenna, completed around Oct. 1, 1972, as initially configured for dual carrier work. During the latter stages of reconfiguration, tests of the transmitter output spectrum using the water load were simultaneously possible. Those data proved the 100-kW transmitter with dual carrier excitation was operating properly, and that transmit-band IMPs were as anticipated from previous tests, or better. In addition, the receive band was checked for possible IMPs. Under no conditions could receive band IMPs be detected. The tangential sensitivity of the instrumentation was -35 dBmW referred to the transmitter output port, through use of the high-power waveguide directional coupler. After consideration is given for the 160 dB of microwave filtering, to be used later, an excess of ~ 55 dB sensitivity was available to detect an IMP of -140 dBmW. Considerable attention was given at this time to possible spurious, harmonic, or other mechanisms to explain the previously observed DSS 14 performance. Most, if not all of the possible complex mechanisms proposed were checked, including sensitivity to maser idler frequencies (fundamental and subharmonic), accomplished in the laboratory. None of these possible mechanisms were identified. On the basis of the above transmitter testing, it was further determined that several standard microwave components (klystron, high-power coupler with associated terminations and cables, harmonic filter, and one type of water

load) were receive band IMP-free at least down to the levels indicated above.

Proceeding with confidence, from the data base that noise burst and intermodulation products at 2290 to 2300 MHz were not sufficiently generated by the 100-kW klystron (<195 dBmW at the TWM input), all four terminations were first tested on Oct. 15, 1972. Nominal test conditions of dual 10-kW carriers with N = 31 were adopted.

The SLH mode showed (via XDS 930 spectrum analyzer) relatively steady −175 ±5 dBmW IMP with NB less than 1 K at the predicted receive band frequency. The water load (Fig. 3) provided comparable performance with the observation that it tended to be mildly microphonic, i.e., shock sensitive (produced NB and presumably transient IMP under vibration). While not ignoring these low level signals, the stronger −135 ±10 dBmW IMP with NB > 500 K in a 1-MHz bandwidth observed on the total antenna system, for the dual 10-kW N = 31 standard conditions adopted, received priority attention. These intermodulation products were, on the average, only a few decibels worse than present at DSS 14, (Fig. 1) even though it was considered that significant structural cleanup had been accomplished at DSS 13 (Fig. 6). A hint of the problems to be later encountered was observed when the flat-plate reflector was used; no repeatable difference in performance between the flat plate mode and the total antenna system mode was detectable.

There were many questions as to whether the flat plate would be an effective switch (Fig. 7) in providing isolation from the antenna reflecting surfaces. Tertiary mechanisms, such as support arm arcing, spillover, diffraction and others, could indeed support the observed intermodulation, in view of the tremendous dynamic range between uplink (+76 dBmW peak) and downlink (−135 dBmW average), which is greater than 200 dB.

In order to provide a high reliability answer to such questions, a more effective switch was employed. The subreflector and quadripod were removed as a unit (Fig. 8). Performance, with or without the flat plate reflector, remained essentially the same with the possibility that the mean level dropped 3 dB (−138 dBmW). Samples of the T_{op} and AGC instrumentation recordings made during this initial period are available in Fig. 9.

By using a manual waveguide switch rotation (SW3 in Fig. 3), the water load was relocated on the unused SW4 port. Performance remained quite poor (~−140 dBmW, 500 K). The waveguide run connecting the 26-m antenna electronics room with the SRO feedcone (SW1 to SW3) was next disassembled, cleaned, acid etched, relapped, and flanges lightly greased according to current DSN standards (Ref. 8). With the exception of startup burn in or "rf processing," and mild microphonics, the waveguide cleanup was considered successful as measured on the relocated water load.

Performance was also significantly improved when radiating out the SRO feed cone, although nowhere near acceptable (−155 dBmW), and quite variable, microphonic, and intermittent. The variability was apparently a function of many things; shock, vibration, solar illumination, rain and polarization, as a minimum accounting.

Because the SRO feedcone polarizer and SW3 were the only waveguide-like components not having undergone cleanup recently, these too were next serviced according to the standard. There was no observable change in performance. Finally, the SRO feedhorn was removed and also serviced.

While the main feedhorn was being serviced it was possible to install a water load on top of the polarizer, in place of the feedhorn. Performance was of the (then acceptable) −175 ±5 dBmW class. By use of a clean 2-m long waveguide, it was further possible to try two other horn radiators on top of the long waveguide, approximately 0.5 m above the feedcone top surface. One horn was low-gain (+6 dBi) while the other was medium-gain (+16 dBi). Both provided intermittent NB and accompanying IMP of the −145 dBmW class until microwave absorber was tried about the feedhorn exterior throat regions. While not eliminating the problem, significant (~15 dB) reduction was observed.

The serviced main feedhorn was reinstalled without change in the −145 dBmW intermittent class performance. The microwave absorber continued to provide significant improvement. One characteristic of all three horns used was that of dominant or single mode excitation. Dominant mode operation is known to diffract significant energy into the rear hemisphere, as a result of untapered E-plane excitation. Power density surveys in amplitude and polarization about the dominant mode SRO feedhorn, and about the hybrid or effectively dual mode SLH confirmed the expected significant density difference as well as expected field orientations. Two main conclusions were drawn from these tests; (1) dominant mode horn diffraction with normally constructed feedcone exteriors is sufficiently strong to excite poorly

bonded metal joints and cause a portion of the microphonic NB/IMP phenomena, but more importantly, (2) a comparison of the power density due to diffraction, and the density to be expected later with hyperboloid illumination shows the hyperboloid illumination to be stronger. Therefore, the feedcone exterior requires sound bonding, independent of horn type, since the hyperboloid illumination dominates.

During all the above testing, the SLH performance remained consistent at the -175 ± 5 dBmW level, on a daily reference basis. It was decided impractical to appropriately bond the SRO feedcone exterior within the available time. An approach utilizing an existing partially welded feedcone, which was to be more fully welded, with the SLH reference horn mounted within, was selected. A simple interior was agreed upon, the only components being a fixed quarterwave plate polarizer and a waveguide connection to the floor interface. The joint between the SLH and the feedcone roof surface was prepared much like a waveguide flange, with approximately five bolts per wavelength, flat, well contacting corrosion-free surfaces, protected with grease. The feedcone doors were insulated rather than welded. Thought was given to the feedcone/reflector interface (an aluminum to steel joint), but nothing practical was devised prior to installation (Fig. 10).

Performance using the prepared exterior feedcone was as expected; NB less than 1 K, with IMP -172 ± 5 dBmW for an extended test period including shock, vibration, solar illumination, and microphonic tests. A second-generation flat plate, with all joints either welded or insulated was then tested, with identical results. It should be noted, however, that such a flat plate test is necessary, but not sufficient. Diffraction and spillover might be possible problems after the quadripod is installed. In view of the large dynamic range involved, the question arises, what would the isolation of this switch be with the quadripod *in situ*?

Although earlier cleanup work on the main reflector surface and quadripod legs had been done, results to date indicated not enough had been accomplished. It was possible, through a parallel effort, to thoroughly bond the subreflector while the new feed cone was being proofed. The vertex plate, beamshaping flange, and to some extent, hardware behind the rim of the flange, were bonded together by welding. This parallel effort eliminated obtaining a pre-calibration on the "as-received" condition of the subreflector. A review of the anticipated power densities on the subreflector and physical condition, compared with earlier experience with feedcone exterior power densities, physical condition, and poor performance, showed that, by a factor of 30 dB, the subreflector would have failed. Figure 11 shows the bonded subreflector being reinstalled in the quadripod; meanwhile testing of the new feed cone is under way (begun around Dec. 7, 1972).

After a high degree of confidence was obtained on the new feed cone, the quadripod was reinstalled (Fig. 2). Questions requiring answers at this point were:

(1) Is the feedcone base to reflector (aluminum to steel) joint adequate under increased illumination stress from the subreflector?

(2) Are the joints between the steel quadripod legs and the aluminum reflector adequate?

(3) Is there sufficient diffracted illumination behind the subreflector to stress the myriad of joints located there which are extremely difficult to bond/insulate/shield?

(4) Is the aluminum tape treatment of reflecting panel joints, found adequate for a single carrier NB solution, sufficient under dual carrier stress?

(5) Are any or all of the above weather or solar illumination dependent (intermittent)?

Reinstallation of the quadripod included retaping of the joints about the reflecting panels which had been removed for access (Note Figs. 6 and 10). Additionally, attempts were made to shield the aluminum to steel interfaces, at both the bases of the quadripod legs and the feedcone base, using aluminum tape. Because of the physical complexity of these joints, many overlapping and/or wrinkled tape joints became evident on visual inspection leading one observer to comment on the probability of overdoing otherwise good practice.

Indeed, a strong indication that this was correct was immediately obtained upon turn-on of the standard conditions; N = 31 dual 10-kW carriers. NB with accompanying IMP at -135 ± 5 dBmW were observed, which had the impact of returning the project to initial poor performance levels. Furthermore, the SLH reference facility was no longer available (used within new feedcone). Wind precluded use of the flat plate at that time. It was decided to remove the complex of tape in the regions surrounding the quadripod leg bases. Performance returned to an encouraging -168 dBmW level. The tape was reinstalled to determine repeatability. The -135 dBmW level repeated. The tape was removed a second time. The

−168 dBmW level repeated. Confidence was gained in two areas; (1) the tape quality indeed was a problem area, and (2) a few (possibly singular) poorly bonded joints can cause essentially the entire problem. In retrospect, team members witnessing all of the above tests are of the judgement that the initial −135 dBmW levels probably represent a saturated effect, i.e., a singular addition to, or subtraction from, a large number of poorly bonded joints goes unnoticed. The strong suggestion here is that a single uncontrolled installation of some peripheral device on the illuminated portion of DSN antenna reflecting surfaces will probably cause an unacceptable noise impulse and intermodulation interference.

Next, tests of dual 5, 10, and 20 kW pairs with N = 31 were conducted. Total operating noise temperature and AGC traces are seen in Fig. 13. A few small intermittents are noticed, increasing with power level. Holding the power level constant at dual 10-kW carriers, other (narrower uplink frequency separation) pairs were tried. N = 48, 75 (Channels 9 + 16 and 13 + 20), 130, 134, and 177 all showed the expected acceptable performance (Fig. 14).

Figure 15, a and b, are less encouraging. Apparently weather, particularly heavy fog or rain, impacts the otherwise good performance severely, and in a complicated way. A suggestion was seen that a totally wetted antenna surface provided a continuous noise-free reflector. An antenna drying out is apparently quite intermittent and noisy. These effects, however, are not yet well understood. Even common environmental effects such as solar radiation remain to be more fully examined.

V. DSS 13 Summary

An approximate 5-month program (3 months at DSS 13) has resulted in much improved understanding of causes and cures for noise impulse and intermodulation phenomena within the DSN. Problems have been observed, identified, and either eliminated or substantially reduced, both within the internal bounded waveguide and external free space wave portions of a typical DSN antenna. Figure 16 summarizes the milestones reached at DSS 13 by the end of this reporting period. While the problems are difficult and dwell on a large number of small details, initially no exotic nor cost prohibitive measures appear necessary. On the other hand, the possibility of a difficult and/or costly follow-on maintenance regimen may be needed, and weather independence may not be possible.

The investigation is not complete. A low-level problem (−175 dBmW) at N = 31, dual 10-kW operation has continually existed. Although this level is acceptable, in the Viking context, given the repeatable decay observed with larger N numbers, the unknown long-term stability of this level is worrisome. Whether this is a waveguide flange or diplexer effect is presently unknown. A high-level problem exists during inclement weather.

VI. Status at Year End

Overall results at DSS 13 by mid-December were such that confidence was building that it would be possible to achieve comparable results on a 64-m antenna, fully appreciating the problems attendant to a much larger structure. Significant unknowns, including the residual intermittence at DSS 13, as well as the scheduled S/X band feed hardware on the 64-m antennas, remained unresolved.

Notwithstanding these difficulties, the outcome of the December 20 meeting with the Viking project was the continued intent to use dual uplinks from each 64-m station. Plans were then made to take advantage of the February-March down time at DSS 14 to make whatever tests and modifications as were judged feasible. In the meanwhile the investigation at DSS 13 was to be completed in a few areas and followed by a long-term evaluation of noise burst and IMP performance.

As of this writing, progress is being made as planned, although recent guidelines suggest that for reasons beyond the control of the DSN, the Viking project plan will be revised to place the dual carrier (from one 64-m station) capability in a mission enhancement classification.

Acknowledgment

The conscientious efforts and unusual contributions from many individuals associated with JPL Sections 331, 332, 333 and 335, as well as Philco Ford, are acknowledged.

References

1. Bathker, D. A., and Brown, D. W., "Dual Carrier Preparations for Viking," in *The Deep Space Network Progress Report*, TR 32-1526, Vol. XI, pp. 146–149. Jet Propulsion Laboratory, Pasadena, Calif., Oct. 15, 1972.
2. Mudgway, D. J., "Viking Mission Support," in *The Deep Space Network Progress Report*, TR 32-1526, Vol. XII, pp. 14–15. Jet Propulsion Laboratory, Pasadena, Calif., Dec. 15, 1972.
3. Jackson, E. B. and Kolbly, R. B., "DSN Research and Technology Support," in *The Deep Space Network Progress Report*, TR 32-1526, Vol. XII, pp. 124–126. Jet Propulsion Laboratory, Pasadena, Calif., Dec. 15, 1972.
4. Smith, R. H., "Dual Carrier," in *The Deep Space Network Progress Report*, TR 32-1526, Vol. XII, pp. 200–201. Jet Propulsion Laboratory, Pasadena, Calif., Dec. 15, 1972.
5. *High Power Transmitters and Dual Carrier Uplink Support for Viking '75*, IOM 3300-72-176, April 17, 1972 (JPL internal document).
6. Jackson, E. B., and Kolbly, R. B., "DSN Research and Technology Support," in *The Deep Space Network Progress Report*, TR 32-1526, Vol. IX, p. 149. Jet Propulsion Laboratory, Pasadena, Calif., June 15, 1972.
7. Jackson, E. B., "DSN Research and Technology Support," in *The Deep Space Network Progress Report*, TR 32-1526, Vol. III, p. 156. Jet Propulsion Laboratory, Pasadena, Calif., June 15, 1971.
8. *Installation Procedure, WR430 Waveguide Assemblies, IP506254A*, Feb. 18, 1972 (JPL internal document).

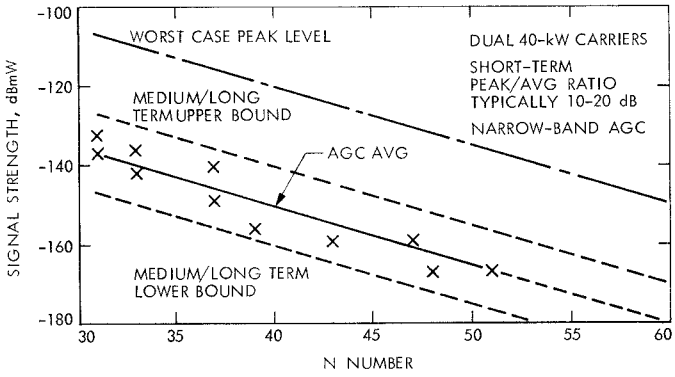

Fig. 1. DSS 14 IMP amplitude as a function of N (1972)

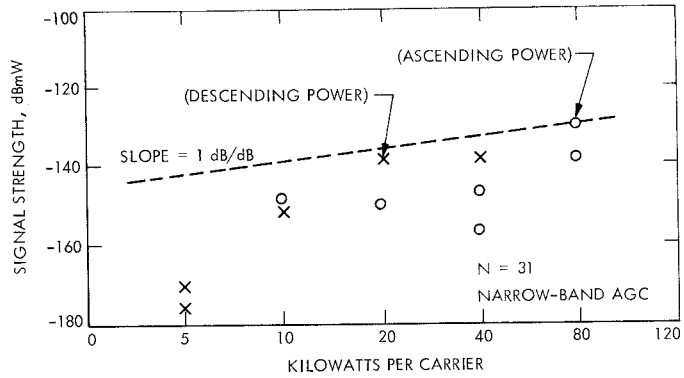

Fig. 2. DSS 14 IMP amplitude as a function of power (1972)

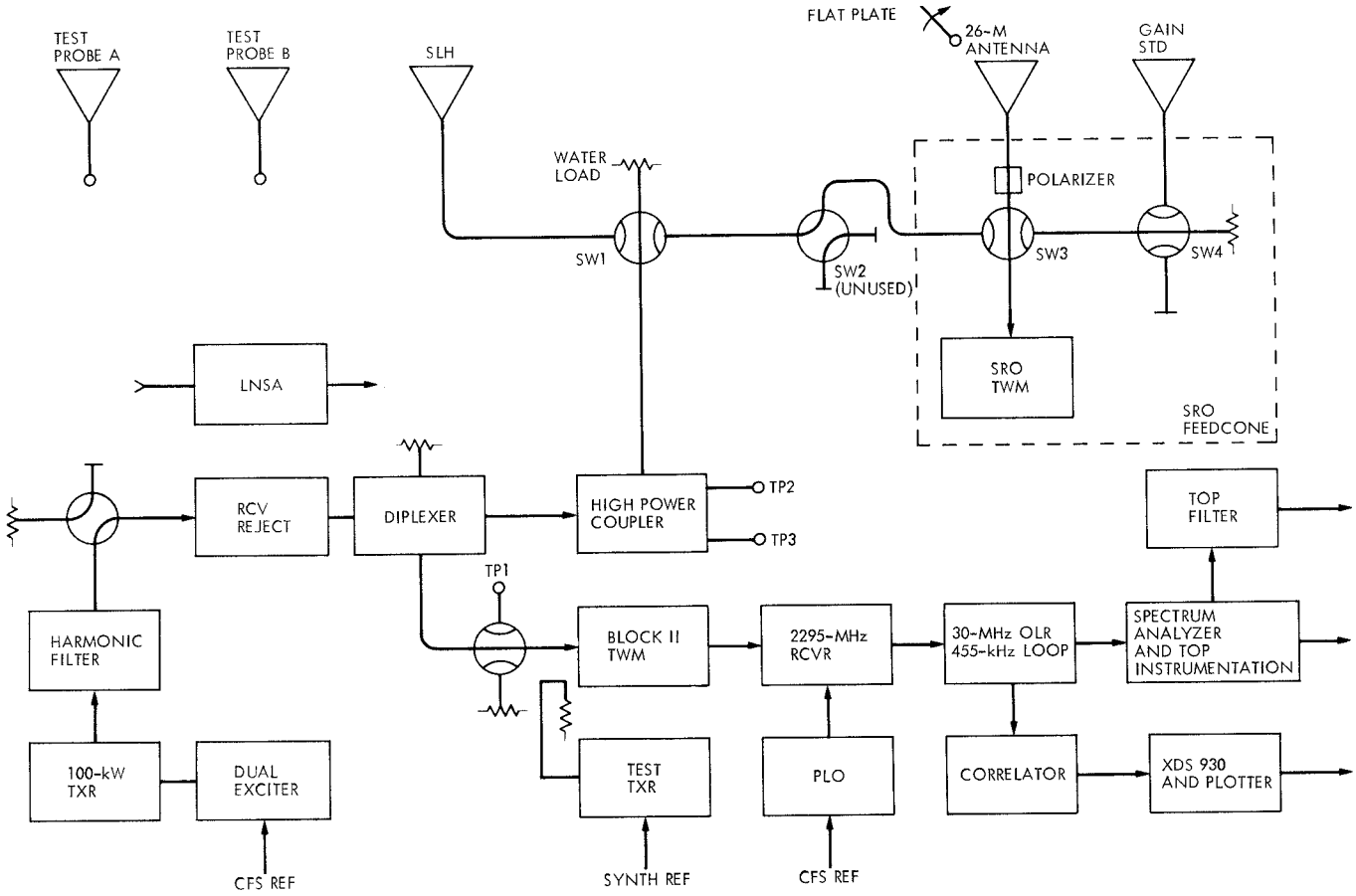

Fig. 3. DSS 13 dual carrier reconfiguration block diagram

Fig. 4. DSS 13 side-looking horn installation

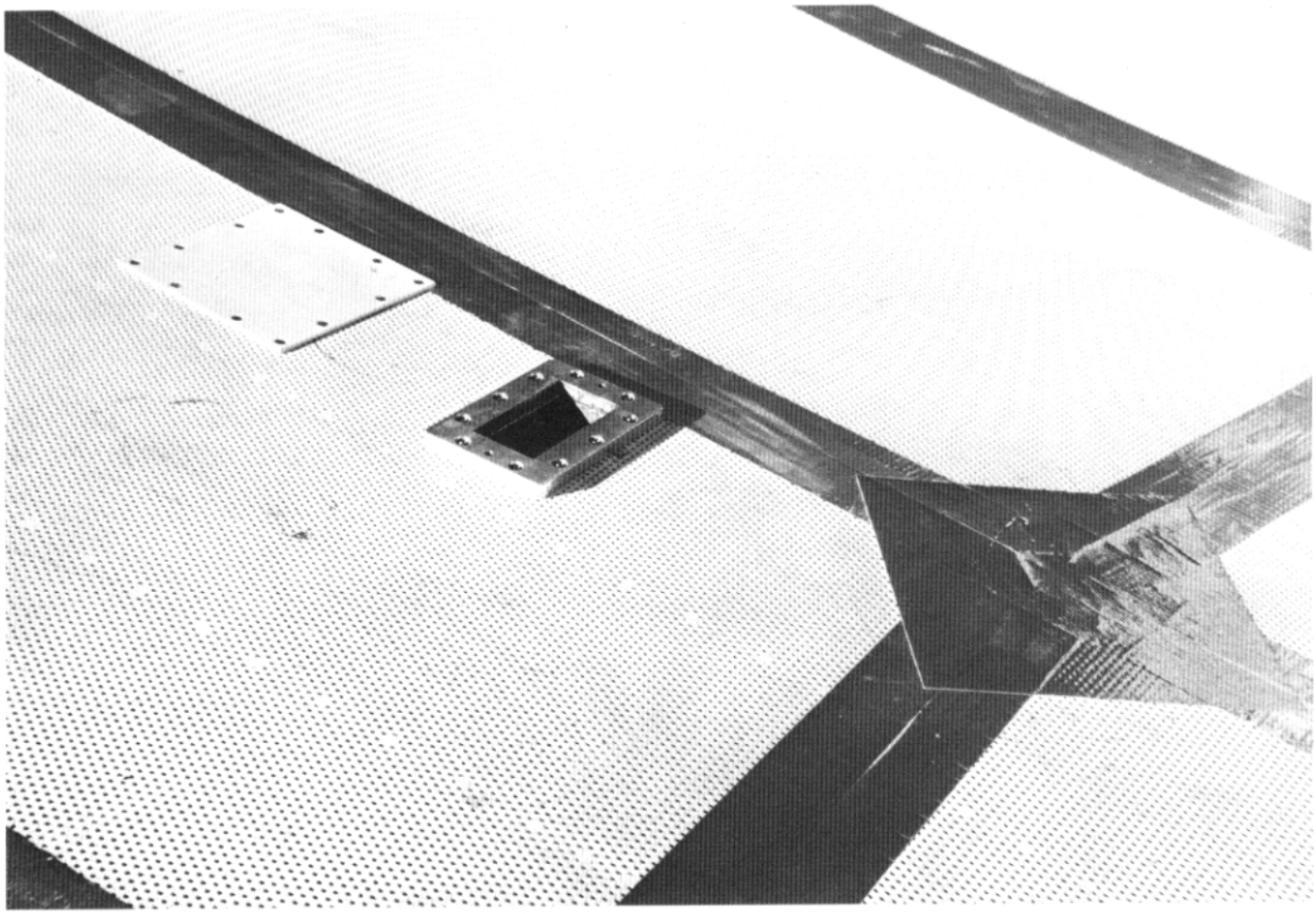

Fig. 5. DSS 13 retaped main reflector and test probes

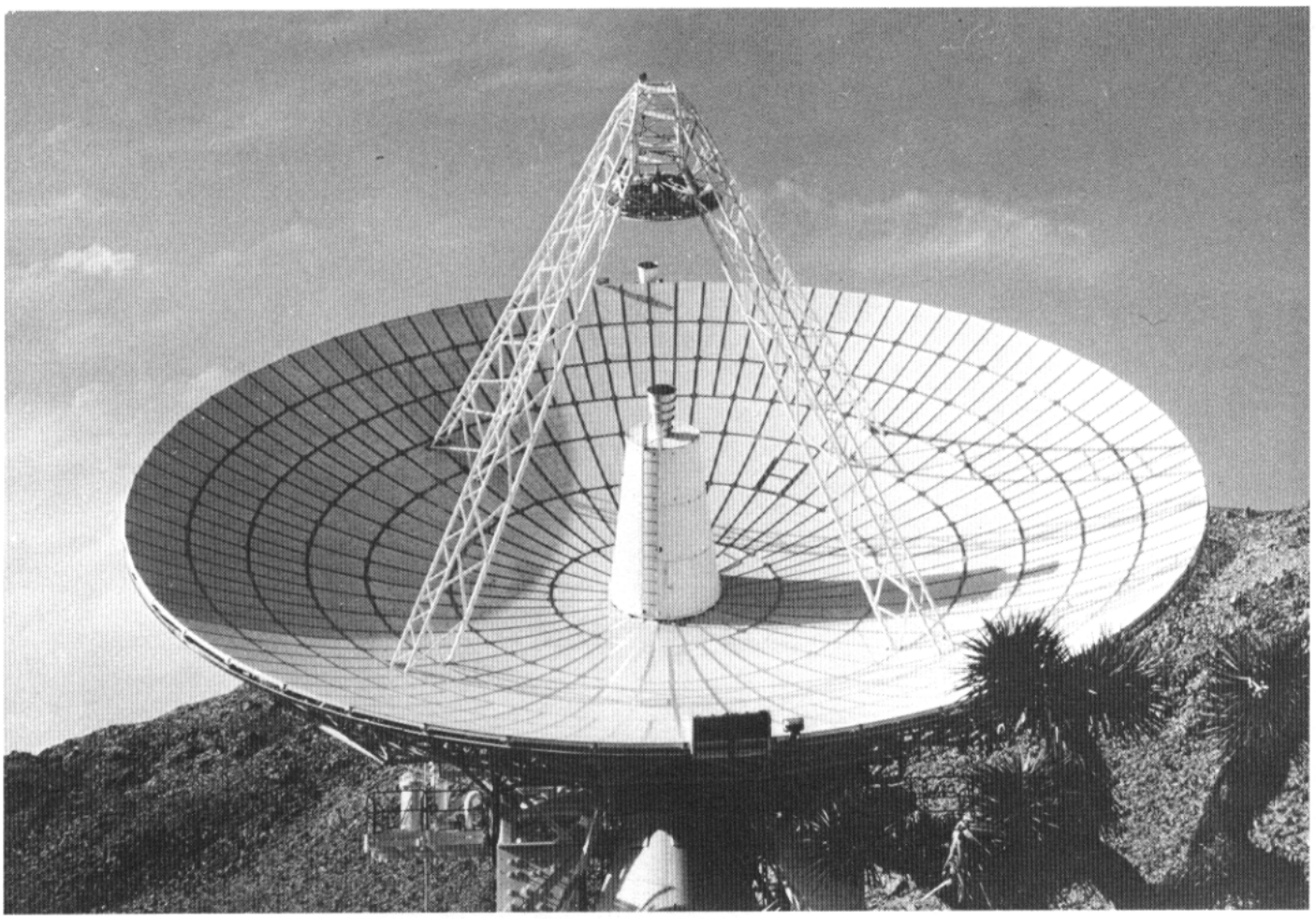

Fig. 6. DSS 13 initial dual carrier configuration

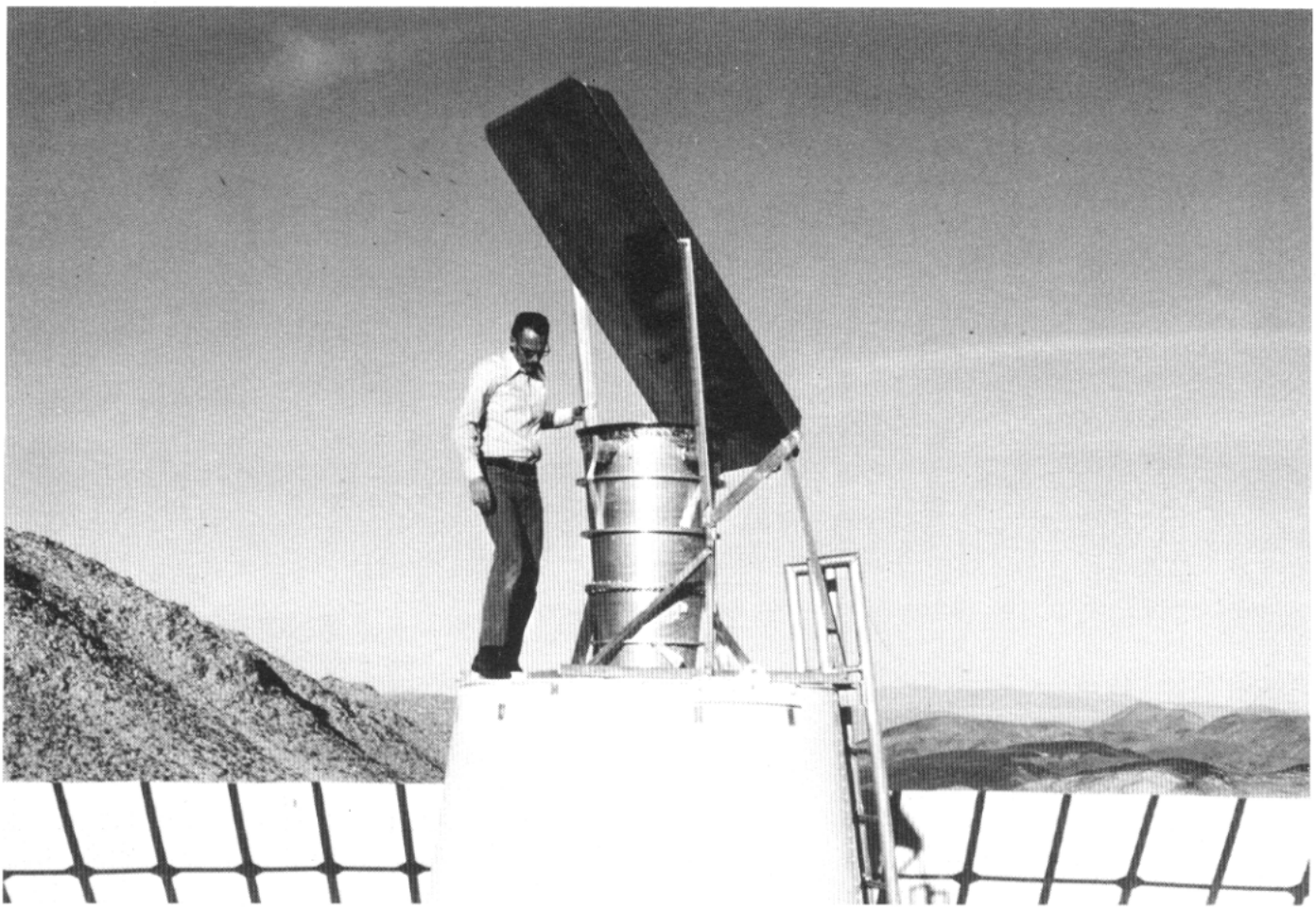

Fig. 7. DSS 13 flat plate reflector on SRO feed cone

Fig. 8. DSS 13 subreflector and quadripod removal

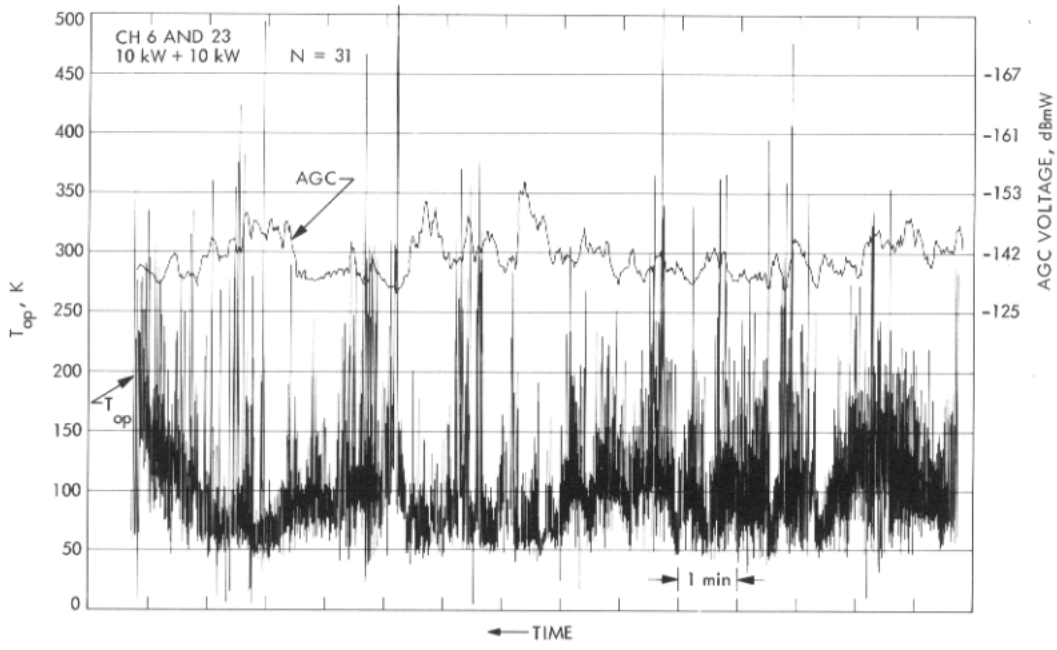

Fig. 9. System temperature and AGC performance, DSS 13 antenna system Oct. 15 to Nov. 1, 1972

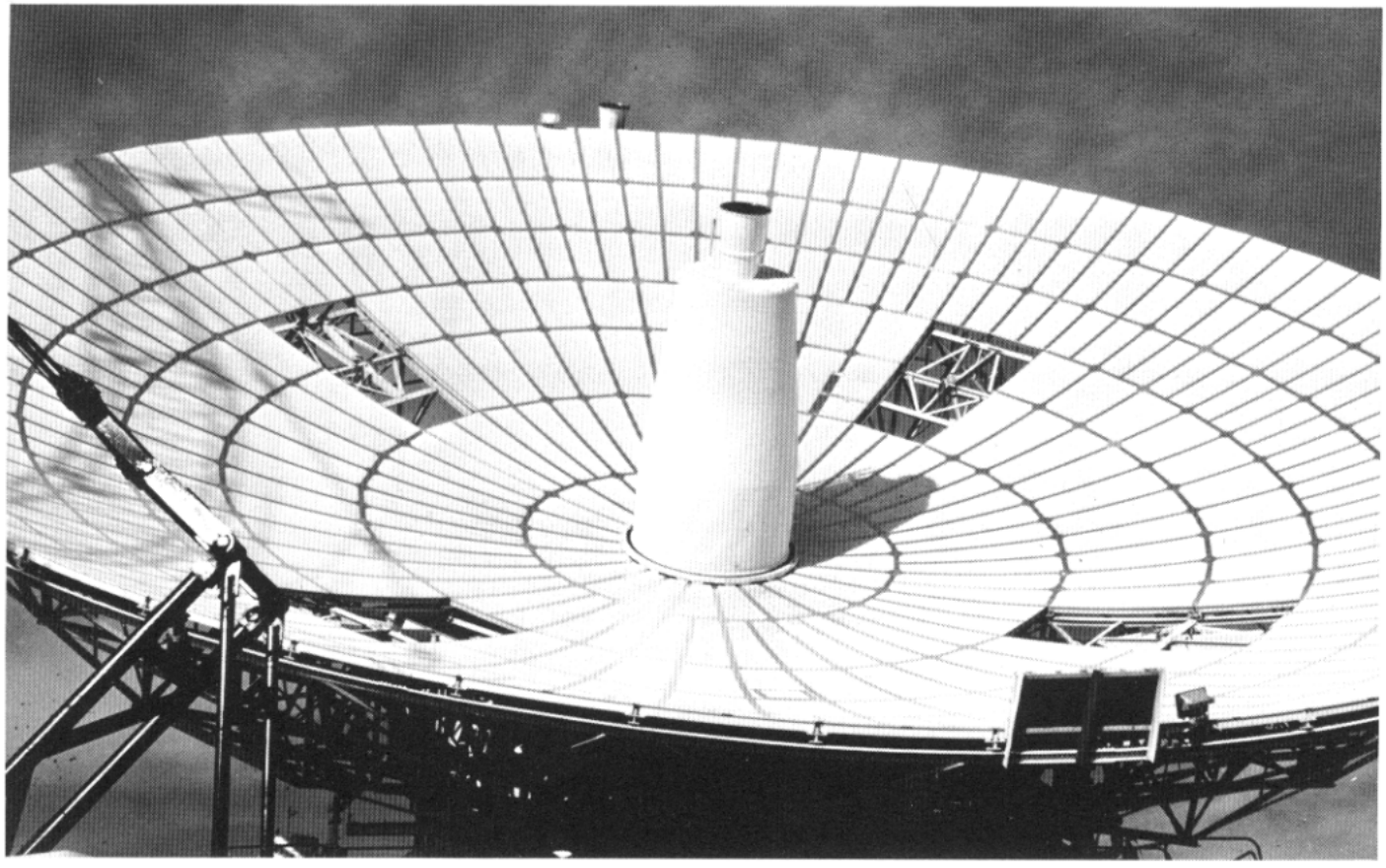

Fig. 10. DSS 13 welded feed cone with SLH horn

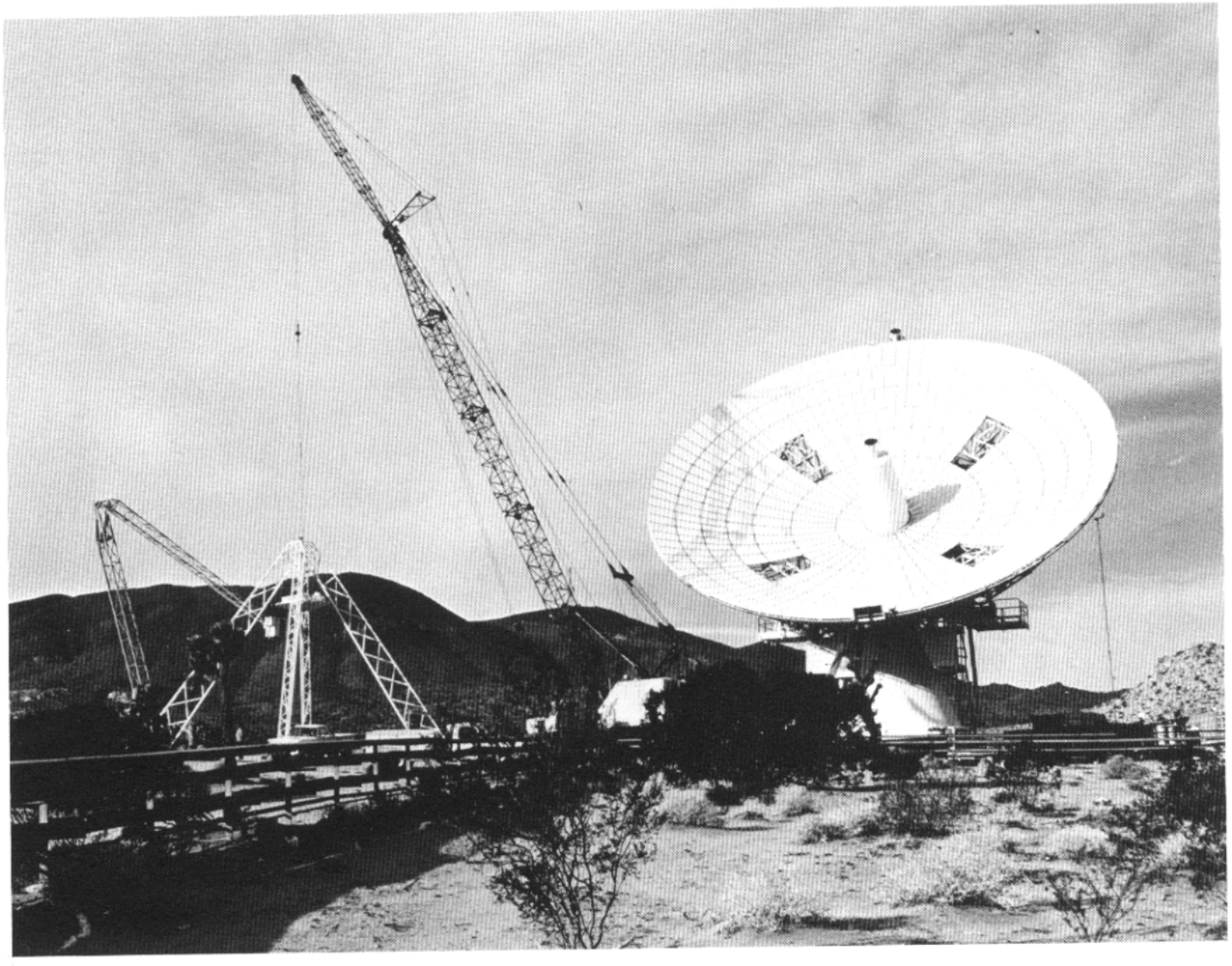

Fig. 11. DSS 13 subreflector installation

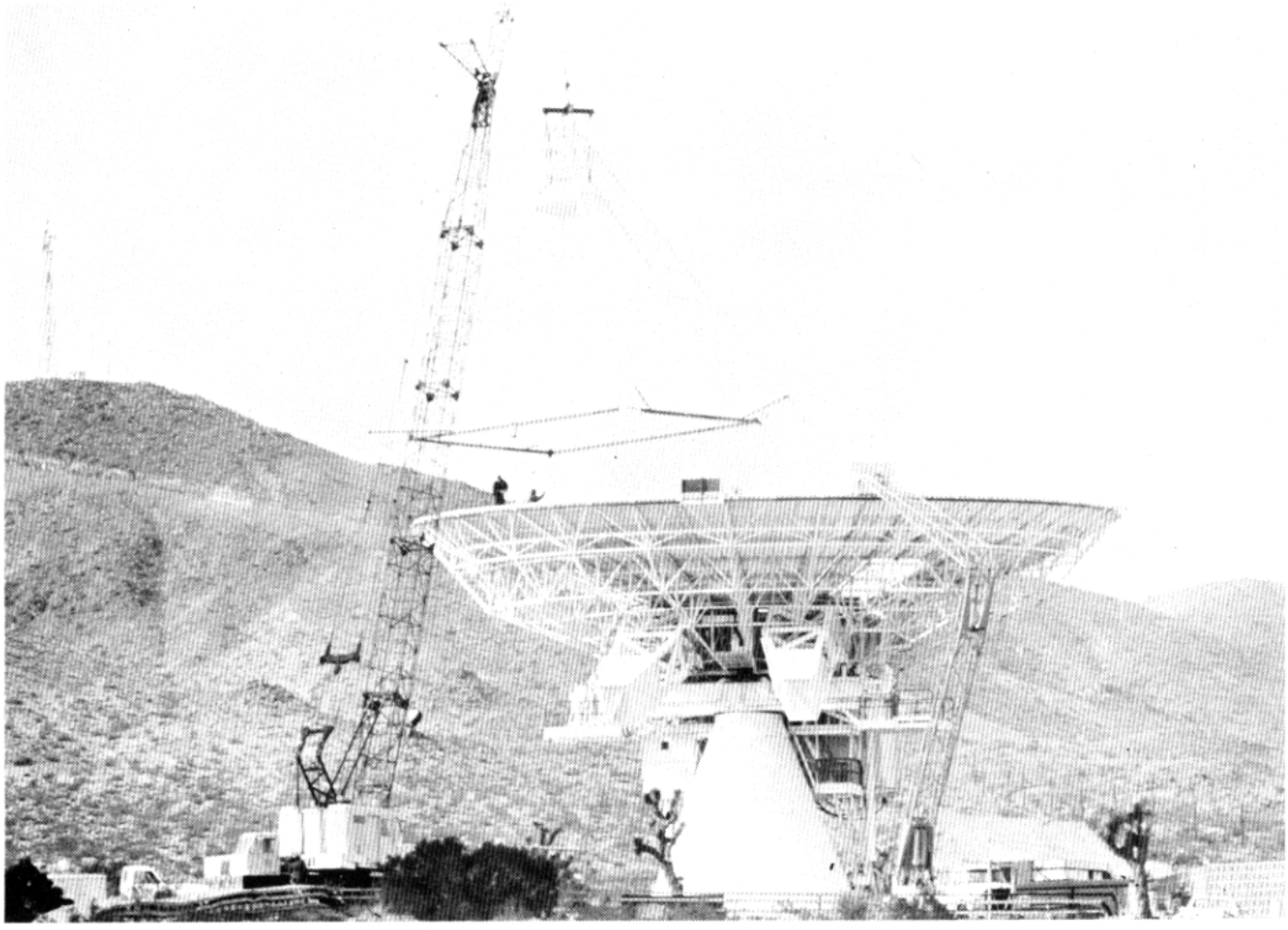

Fig. 12. DSS 13 quadripod installation

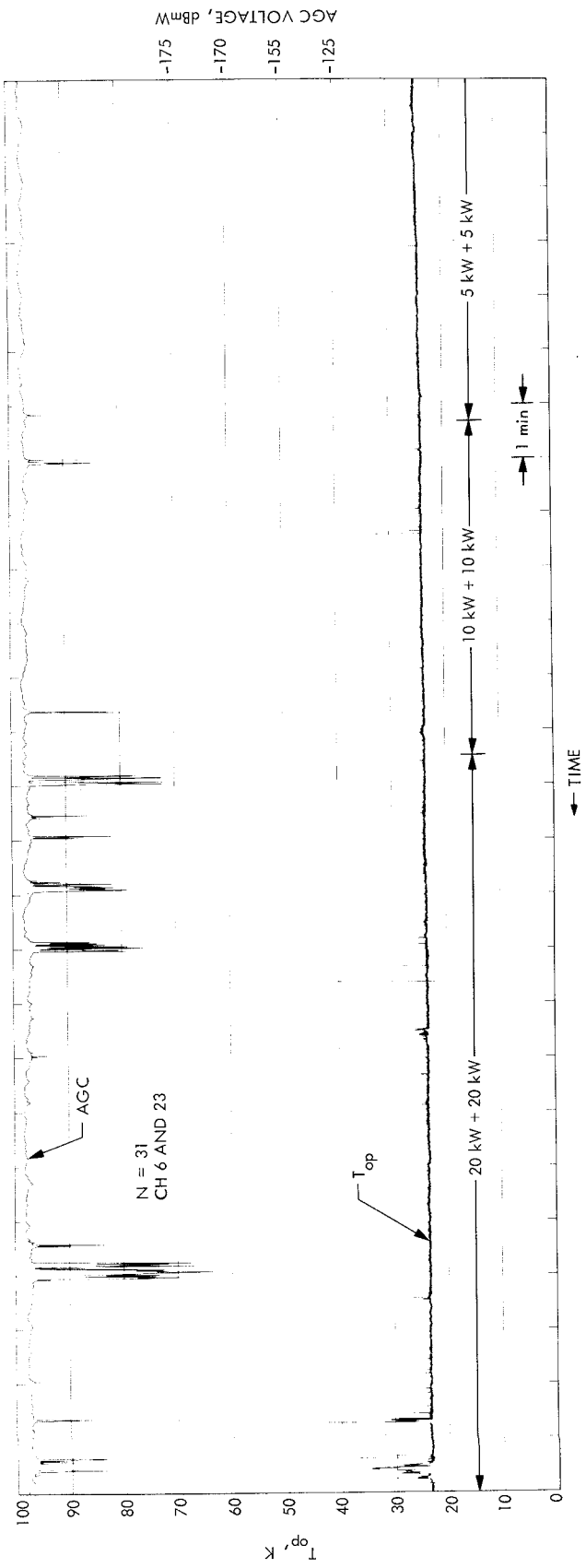

Fig. 13. System temperature and AGC performance, DSS 13 antenna system, Dec. 7, 1972

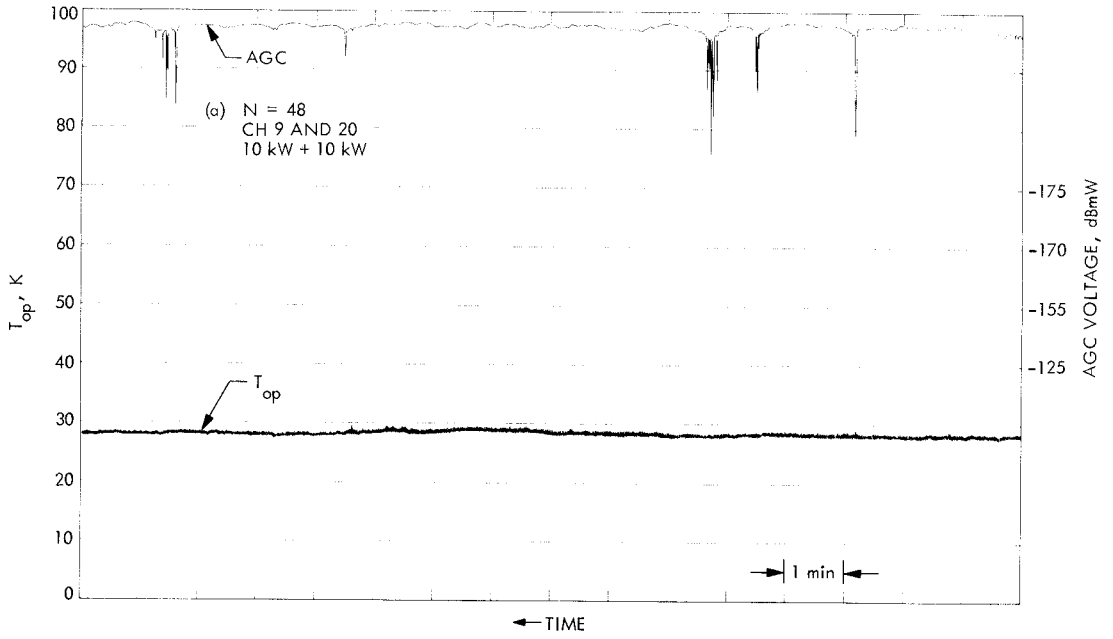

Fig. 14. System temperature and AGC performance as functions of N, DSS 13 Antenna System, Dec. 7, 1972

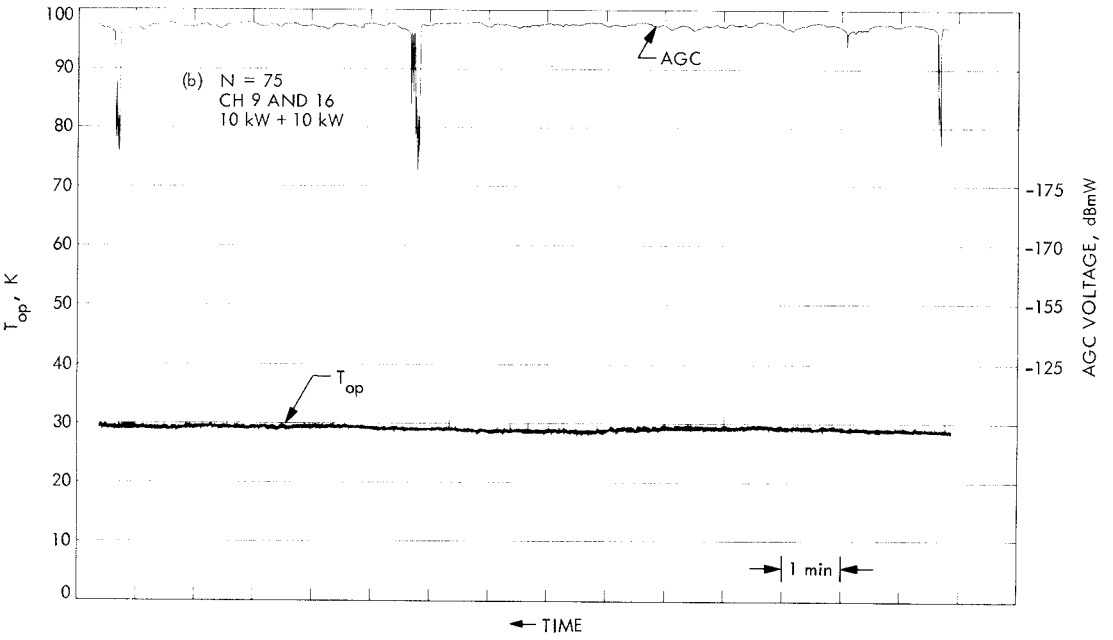

Fig. 14 (contd)

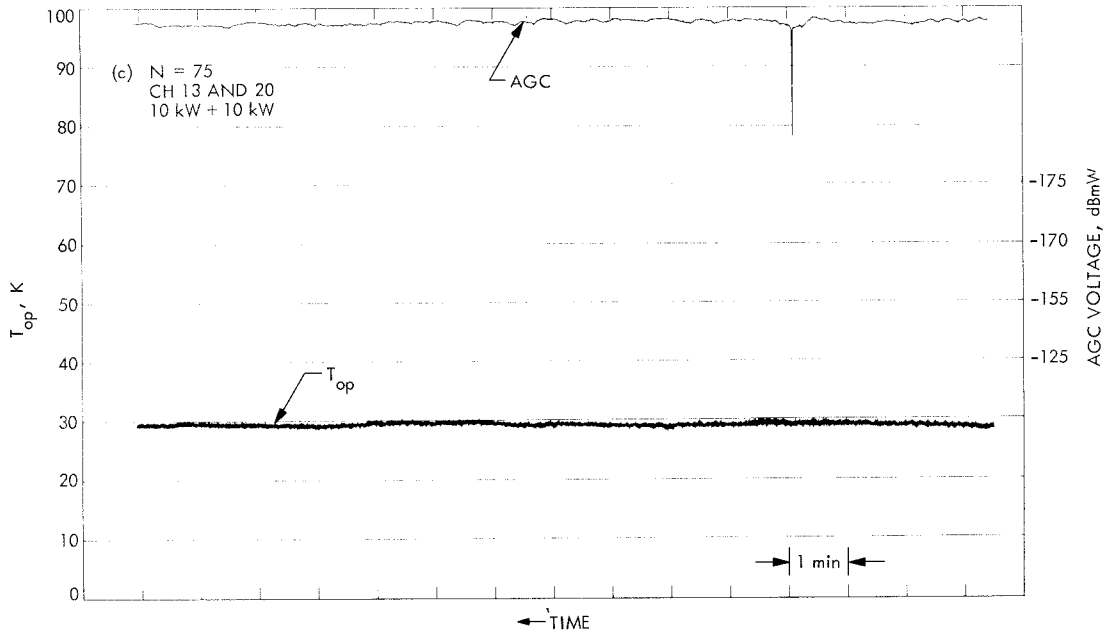

Fig. 14 (contd)

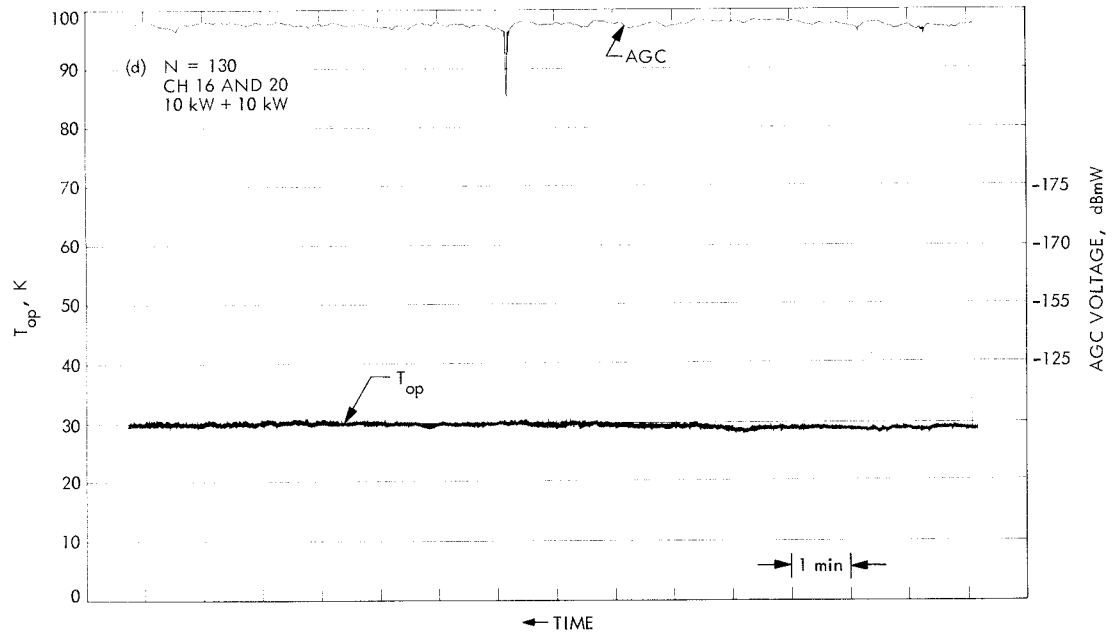

Fig. 14 (contd)

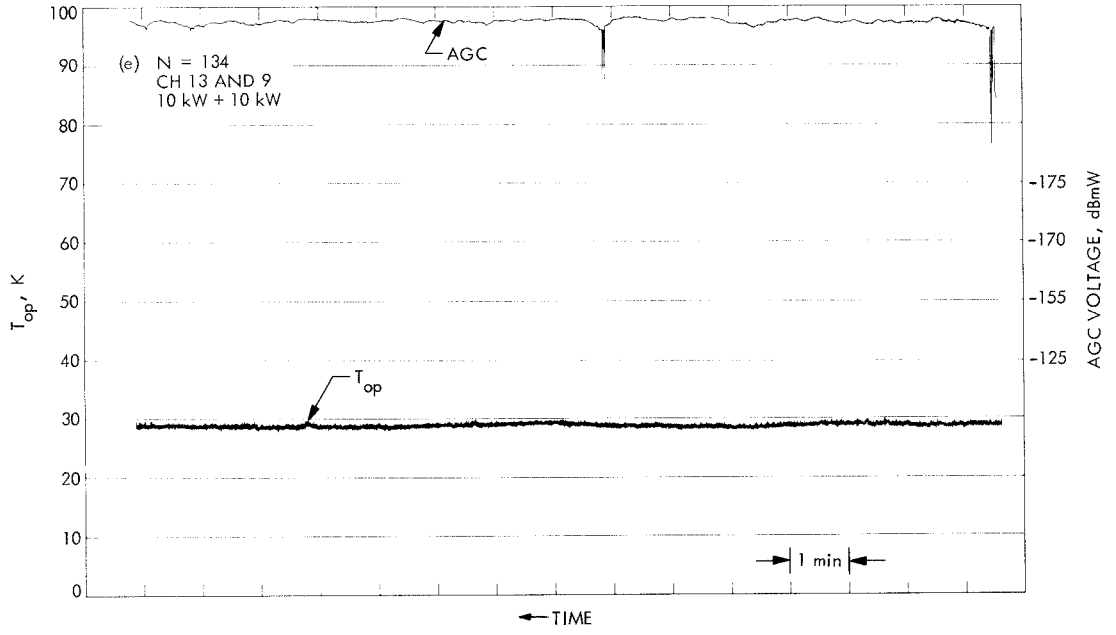

Fig. 14 (contd)

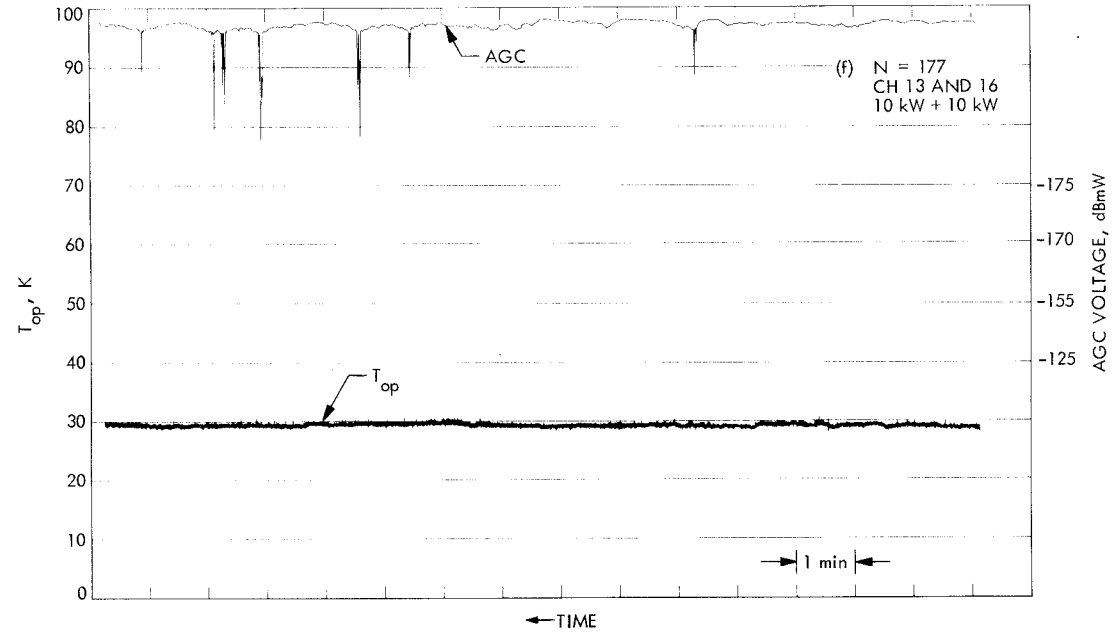

Fig. 14 (contd)

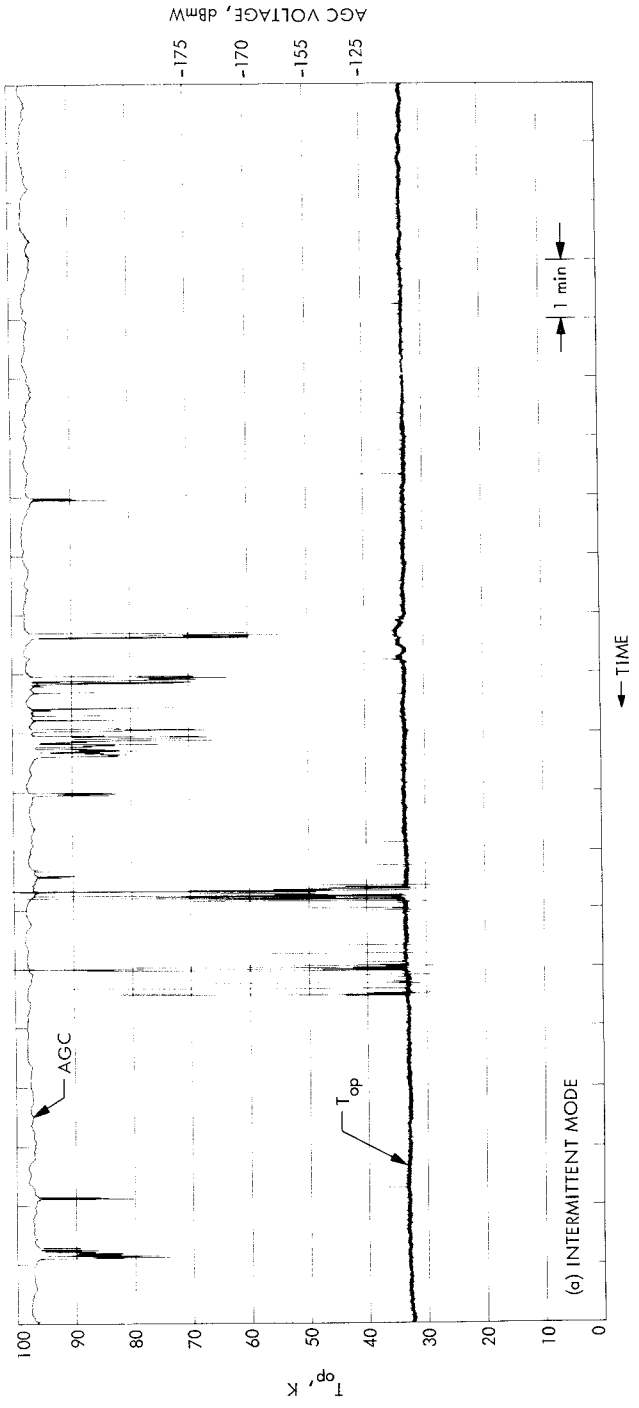

Fig. 15. DSS 13 antenna system temperature and AGC performance on Dec. 8, 1972
(a) during intermittent mode (b) during probable weather effects

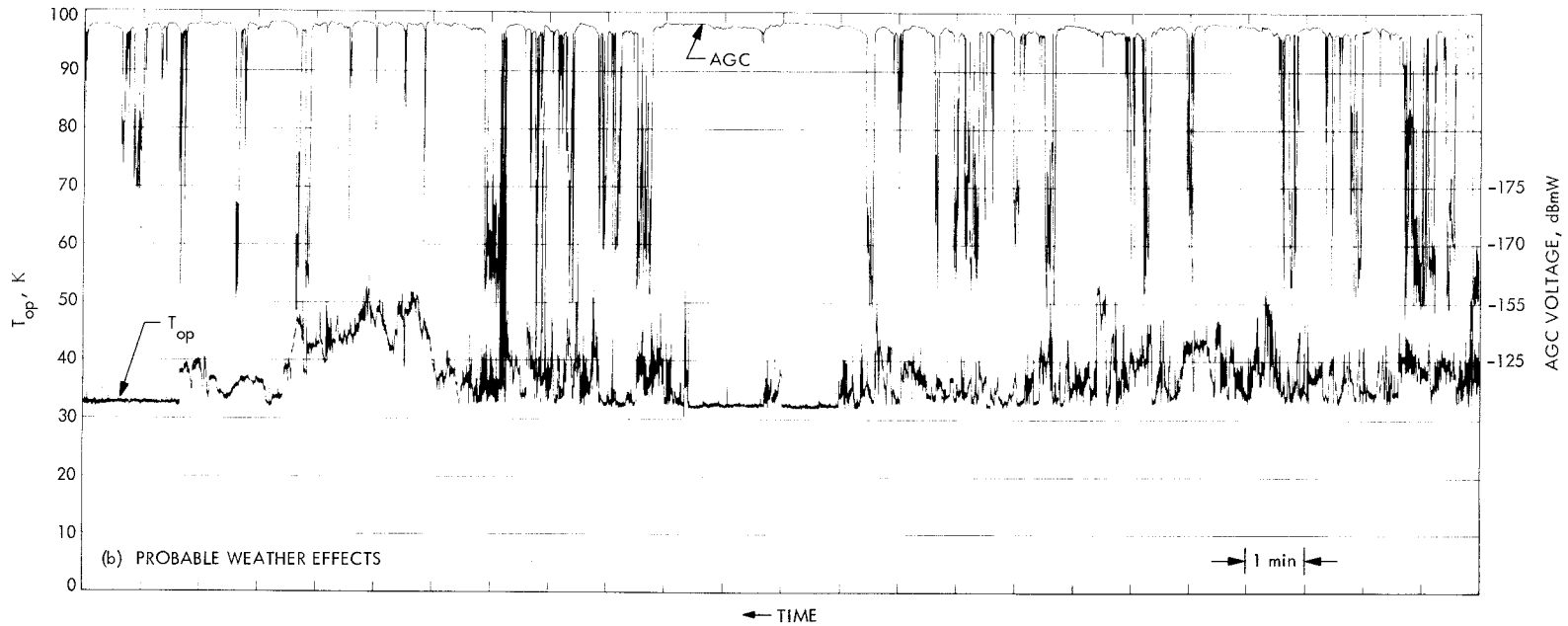

Fig. 15 (contd)

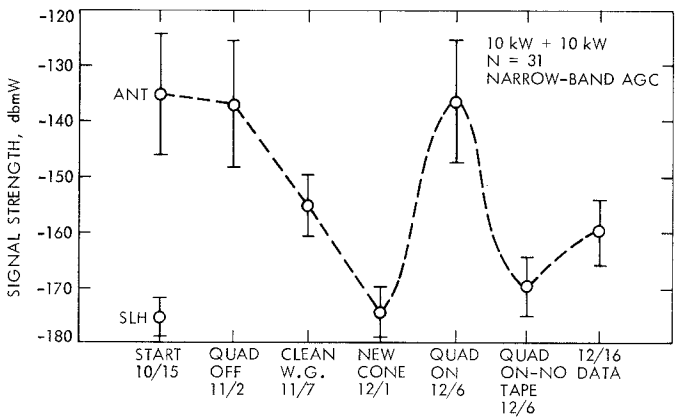

Fig. 16. DSS 13 milestones of IMP performance, 1972